DARU Journal of Pharmaceutical Sciences (2019) 27:49–58
https://doi.org/10.1007/s40199-019-00241-y

RESEARCH ARTICLE

Iron oxide nanoparticulate system as a cornerstone in the effective delivery of Tc-99 m radionuclide: a potential molecular imaging probe for tumor diagnosis

Mohamed M. Swidan[1] · Omnya M. Khowessah[2] · Mohamed Abd El-Motaleb[1] · Ahmed Abd El-Bary[2] · Mohamed T. El-Kolaly[1] · Tamer M. Sakr[3,4]

Received: 16 October 2018 / Accepted: 7 January 2019 / Published online: 31 January 2019

Abstract

Background The evolution of nanoparticles has gained prominence as platforms for developing diagnostic and/or therapeutic radiotracers. This study aims to develop a novel technique for fabricating a tumor diagnostic probe based on iron oxide nanoparticles excluding the utilization of chelating ligands.

Methods Tc-99 m radionuclide was loaded into magnetic iron oxide nanoparticles platform (MIONPs) by sonication. ^{99m}Tc-encapsulated MIONPs were fully characterized concerning particles size, charge, radiochemical purity, encapsulation efficiency, in-vitro stability and cytotoxicity. These merits were biologically evaluated in normal and solid tumor bearing mice via different delivery approaches.

Results ^{99m}Tc-encapsulated MIONPs probe was synthesized with average particle size 24.08 ± 7.9 nm, hydrodynamic size 52 nm, zeta potential -28 mV, radiolabeling yield 96 ± 0.83%, high in-vitro physiological stability, and appropriate cytotoxicity behavior. The in-vivo evaluation in solid tumor bearing mice revealed that the maximum tumor radioactivity accumulation (25.39 ± 0.57, 36.40 ± 0.59 and 72.61 ± 0.82%ID/g) was accomplished at 60, 60 and 30 min p.i. for intravenous, intravenous with physical magnet targeting and intratumoral delivery, respectively. The optimum T/NT ratios of 57.70, 65.00 and 87.48 were demonstrated at 60 min post I.V., I.V. with physical magnet targeting and I.T. delivery, respectively. These chemical and biological characteristics of our prepared nano-probe demonstrate highly advanced merits over the previously reported chelator mediated radiolabeled nano-formulations which reported maximum tumor uptakes in the scope of 3.65 ± 0.19 to 16.21 ± 2.56%ID/g.

Conclusion Stabilized encapsulation of ^{99m}Tc radionuclide into MIONPs elucidates a novel strategy for developing an advanced nano-sized radiopharmaceutical for tumor diagnosis.

Keywords Magnetic iron oxide nanoparticles · Tc-99 m radionuclide · Chelator free radiolabeling · Encapsulation · Tumor delivery · Tumor diagnosis

✉ Mohamed M. Swidan
dr_swidan@yahoo.com

✉ Tamer M. Sakr
Tamer_sakr78@yahoo.com

[1] Labeled Compounds Department, Hot Labs Center, Egyptian Atomic Energy Authority, PO13759, Cairo, Egypt

[2] Pharmaceutics and Industrial Pharmacy Department, Faculty of Pharmacy, Cairo University, PO11562, Cairo, Egypt

[3] Radioactive Isotopes and Generator Department, Hot Labs Center, Egyptian Atomic Energy Authority, PO13759, Cairo, Egypt

[4] Pharmaceutical Chemistry Department, Faculty of Pharmacy, Modern Sciences and Arts University, 6th October City, Egypt

Introduction

The tumor targeting ability of nanoparticles (NPs) as drug delivery vehicles is derived from their tunable small size (10-100 nm) [1]. Recently, radionuclide imaging based nanoparticles has been drawing in extraordinary enthusiasm for preliminary research and clinical application [2]. Chelator mediated radiolabeled NPs have been commonly developed and investigated in many researches as diagnostic and/or therapeutic agents [3, 4]. But unfortunately, there are some limitations are stated during the development of chelator mediated radiolabeled NPs such as the multifaceted nature of coordination chemistry, probable pharmacokinetics change in carrier

behavior and possible radionuclides detachment [5, 6]. Herein, it is important to navigate the requirements for designing a straightforward yet promising strategy for the future aspect of radiolabeled nanoparticles development. The developing idea of intrinsically chelator free radiolabeled nanoparticles could be potentially magnified by utilizing strategies such as encapsulation, physisorption, isotope exchange, and particle beam or reactor activation [7]. The encapsulation strategy provides advanced control on transmetallation over metal chelation and furthermore stays away from the need of developing novel ligands for various imaging agents and applications [8]. As the stabilized encapsulation can protect the payload entity from the biological interaction, it can demonstrate prober in-vivo stability [1, 9]. The efficient radionuclide delivery to tumor tissues requires several critical design issues that must be accomplished in the final formulation [10–12]. For instance, the successful radiolabeled probe should demonstrate high radionuclide encapsulation capacity, low cytotoxic behavior, sufficient metabolic stability and appropriate pharmacokinetic profile regarding the immediate accumulation in the desired target organ.

The aim of the current research is the development of a novel technique for fabricating a tumor diagnostic probe based on iron oxide nanoparticles encapsulated with Tc-99 m radionuclide without the use of chelating ligands. This strategy incorporated the radionuclide with IONPs in one basic structure where particles size, charge, radiochemical purity, encapsulation efficiency; in-vitro stability and cytotoxicity were evaluated. Then their merits were biologically evaluated in normal and solid tumor bearing mice via several delivery routes (intravenous (I.V.), I.V. with the aid of permanent magnet localized at the tumor region and intratumoral injection (I.T.)).

Experimental

Materials

The reagents were commercially accessible and utilized as delivered without encourage refining. All steps concerning the solution preparation were performed using bidistilled water. Ferric chloride hexahydrate ($FeCl_3.6H_2O$, 99%, M.Wt. 270.33 g/mol), ferrous chloride tetrahydrate ($FeCl_2.4H_2O$, 98%, M.Wt. 198.83 g/mol), PEG-6000, acetone (CH_3COCH_3, M.Wt. 85.08 g/mol), aqueous ammonia (NH_4OH, 57.6 wt.%), Dimethyl sulfoxide; DMSO ($(CH_3)_2SO$, M.Wt. 87.13 g/mol), and crystal violet ($C_{25}H_{30}N_3Cl$, M.Wt. 407.98 g/mol) were applied from Sigma Aldrich company, St. Louis, Mo., USA. Technetium-99 m was obtained as pertechnetate elute from $^{99}Mo/^{99m}Tc$ generator which was acquired from the Egyptian Atomic Energy Authority (EAEA). Human lung fibroblast normal cell line (WI-38 cells) was acquired from VACSERA Tissue Culture Unit, Egypt. A planed, spherical neodymium magnet (10 mm in diameter with 100 mT power) was acquired from Ningbo Daxie Magnetic Co., Ltd. (China). Whatman paper No.1 sheets were obtained from Merck (Darmstadt, Germany).

Equipment

The images of Transmission Electron Microscopy, TEM, (Ted Pella, Redding, CA, USA) were acquired in order to detect the particle size. Dynamic light scattering (DLS) technique (Brookhaven Instruments Corp. (BIC), USA) was used for the determination of hydrodynamic diameter (d_{hyd}). Photo correlation spectrometer, PCS, (Zetasizer Nano™, Beckman Coulter, Miami, FL, USA) was used to determine the zeta potential. Fourier transform infrared (FT-IR) instrument (Mattson Instruments, Inc., New Mexico, USA) was utilized to ensure the prober group functionalization. A NaI (Tl) γ-ray scintillation counter (Scaler Ratemeter SR7 model, UK) was utilized to detect the radioactivity. High-powered sonicator (Q1375 with booster probe, 20 kHz, chemistry RG Consultant Inc., Quebec, Canada) was employed for the encapsulation process.

Animal model

The entire animal study fitted with the ethical rules and the principles for the animal care that are proposed by the animal ethics committee (EAEA/2018/174), EAEA. This committee follows the rules stated by the European Community guidelines for the use of the experimental animals. Normal Swiss albino mice and solid tumor bearing mice of weight 25–45 g were obtained from The National Research Center, Egypt. They were stayed in gatherings of six and free access to food and water. They were retained at a steady room temperature with a 12 h light/dim turning.

Methods

Development of iron oxide nanoparticles

Magnetic Iron oxide nanoparticles (MIONPs) were developed by a modified co-precipitation method [13, 14]. Ferric chloride and ferrous chloride at a molar ratio 2:1 were dissolved in 20 mL deionized water and then 20 mL of 10% PEG was added and mixed together. The solution was bubbled with Nitrogen gas to forestall the unwanted oxidation, warmed to 50 °C while the stirring process was continued. At this point, ammonia solution was added dropwise till the pH of the mixture achieved 10. Then, the reaction mixture was exposed to vigorous stirring at 50 °C for 1 h. The produced Fe_3O_4-PEG

precipitate was removed from the solution via magnetic decantation. The black precipitate was collected then washed many times with bidistilled water to get neutral pH.

Characterization of MIONPs

The size and morphology of MIONPs were examined by TEM where samples of MIONPs (spot of diluted aqueous suspension) were putted on a carbon-covered copper grid and then the solvent was left to vanish at room temperature. The hydrodynamic diameter (d_{hyd}) and size distribution of MIONPs in their aqueous suspensions were estimated using DLS technique. The charge of the formulation, zeta potential, was measured by PCS at room temperature. The FT-IR spectrum (scanning range 4000–400 cm^{-1}) was utilized to determine the functional groups and the proper attachment of the polymer to the MIONPs.

Radiolabeling through encapsulation approach

Under sonication, the MIONPs were redispersed into 5 mL H_2O then 200 μL of a fresh pertechnetate elute, TC-99 m, (8.07 MBq) was added. The sonication time was studied at different time intervals to obtain well dispersed nanoparticles encapsulated with TC-99 m radionuclide. The encapsulated entities were then isolated from non-encapsulated ones by precipitation with the assistance of external magnet (magnetic decantation). The supernatant was expelled and the precipitated ^{99m}Tc-encapsulated MIONPs were washed a few times with deionized water. The radiolabeling yield of ^{99m}Tc-encapsulated MIONPs after magnetic decantation was calculated as follow:

$$\text{Radiolabeling yield} = \frac{\text{radioactivity in the precipitate}}{[\text{activity in the supernatant} + \text{activity in theprecipitate }]} \times 100$$

The formation of ^{99m}Tc-encapsulated MIONPs and radiolabeling yield were confirmed by paper radiochromatography (PC) where acetone was used as a mobile phase. Furthermore, the radiolabeling yield of ^{99m}Tc-encapsulated MIONPs was confirmed by electrophoresis technique which is performed at voltage of 300 V for 1 h using normal saline (0.9% *w*/*v* NaCl solution) as electrolytes source solution.

Encapsulation efficiency (in-vitro release study)

The encapsulation efficiency of ^{99m}Tc-encapsulated MIONPs was evaluated up to 8 h where the encapsulated and leached entities were separated by magnetic decantation. The percent of each entity (encapsulated and leached) was estimated at predetermined time points using radiochromatographic techniques as pointed above.

In-vitro stability study

The in-vitro stability of ^{99m}Tc-encapsulated MIONPs formulation was estimated for ensuring that the radiolabeling process could withstand the physiological conditions [15–17]. Exactly 0.1 mL of the final preparation of ^{99m}Tc-encapsulated MIONPs was incubated with 0.9 mL saline buffer (pH = 7.2) for 24 h at 37 °C. Radiolabeling yields were determined by the radiochromatographic methods that are described above at different time intervals. The same technique with the same conditions was repeated using fresh mice serum instead of saline buffer.

In-vitro cytotoxicity study

WI-38 cells (human lung fibroblast normal cell line) were cultivated in 96-well plates where each well contained a cell concentration of 1×10^4 cells in 100 μl of growth medium. After 24 h of seeding, MIONPs fresh samples with different concentrations were added. Serial two-fold dilutions about the examined samples had been value added in conformity with convergent cell monolayers that are allotted into 96-well flat-bottomed microtiter plates (Falcon, NJ, USA) employing a multichannel pipette. The microtiter plates had been incubated at 37 °C into a humidified incubator together with 5% CO_2 for duration of 48 h. Three wells had been used for each concentration regarding the checked samples. After the incubation period, the viable cells yields had been determined colorimetry using crystal violet stain (1%) in which the absorbance of the plates had been measured employing a check wavelength of 490 nm.

In-vivo biological studies

The in-vivo preliminary evaluation was evaluated in four groups of normal and solid tumor bearing mice (A, B, C, and D). In group A, the biodistribution studies of the ^{99m}Tc-encapsulated MIONPs preparation in normal mice were carried out. Exactly, 15 μl having 4.5 MBq of the radiolabeled NPs was I.V. injected in the tail vein of every mouse. The in-vivo distribution pattern of the prepared formulation was evaluated in solid tumor bearing mice where 15 μl (4.5 MBq) of the formulation was injected via the tail vein for group B. A permanent magnet was localized at the tumor region on the right thigh for group C after I.V. injection. In group D, the intratumoral injection of 15 μl (4.5 MBq) of the radiolabeled NPs was carried out by the direct injection through the right thigh (solid tumor tissue) of each mouse. For each group, the mice were anaesthetized then weighed at 30, 60 and 120 min post-injection (p.i.). All organs as well as tumor tissues were

immediately extracted, flushed with saline, weighed and their radioactivity was estimated using a well type NaI gamma counter where the background was excluded. The percentage injected activity per gram of tissues (%ID/g) was estimated and the tissue uptakes were statistically evaluated by one way ANOVA test.

Results and discussion

Development and characterization of the MIONPs

Iron oxide nanoparticles were developed through aging stoichiometric reaction of ferrous and ferric chlorides in aquatic media. PEG was included during the nanoparticles synthesis to decorate them in order to generate a repulsive force between the particles and protect them from aggregation.

TEM analysis revealed that spherical MIONPs were developed with average size in the scope of 24.08 ± 7.9 nm (Fig. 1a). DLS measurements uncovered that the d_{hyd} across IO-PEG NPs was around 52 nm (Fig. 1b). This indicates the impact of the decorating polymer coating on the 24 nm iron oxide cores.

The hydrodynamic sizes of the synthesized MIONPs were larger than those indicated by their TEM images. This may be attributed to the hydrogen bond formation between the hydroxyl groups of surface coating polymeric chains and the water adsorbed on nanoparticles [18]. These results affirm the authoritative PEG coating onto the IO-NPs with little level of aggregation could occur in aqueous colloidal media [19].

The MIONPs surface charges were estimated through the determination of zeta potential. The binding of PEG generates highly negative surface charge (−28 mV at pH 7) which results in developing electrostatic repulsive force between IO-PEG NPs and hence, stabilized formulation was accomplished [20].

The prober coating of PEG on the surface of MIONPs was further confirmed and demonstrated by FT-IR spectroscopic analysis (Fig. 2). The FT-IR spectra of PEG coated MIONPs revealed an intense absorption peak at 588 cm^{-1}, which may be assigned to Fe-O bond vibrational band [21], and refers to the formation of MIONPs [22]. The broad band at 3283 cm^{-1} was due to OH stretching while the peaks at 1636 cm^{-1} and 1454 cm^{-1} are corresponding to stretching vibration of C=O and bending vibration of OH of PEG [18, 23]. Thus, the zeta potential and FTIR results had come to affirm that IO-NPs had been probably decorated by PEG through van der waals force interaction.

Radiolabeling of MIONPs

There are some major requirements in the radiolabeling process of NPs [24]. These requirements can be stated as i) irreversible binding of radionuclides to NPs to avoid the undesired localization in non-target organs ii) the processing technique should be time limited to decrease the radiation hazard risks iii) the characteristic and structural behavior of the NPs should not be changed during the labeling process iv) highly stable radiolabeling yield should be achieved to allow further in-vivo and in-vitro studies. Recent researches have focusing on growing more dependable chelator free radiolabeling methods. So, it could completely take the benefits of the exceptional physiochemical characteristics of the well-chosen nanoparticle platforms for radiolabeling. Furthermore, this era provides a simpler, speedier, and more significantly radiolabeling technique [5]. Based on the previous findings, IO-NPs (one of the current nano-platforms in medicine) [25] were radiolabeled with Tc-99 m through chelator free approach. Tc-99 m radionuclide is the most commonly administrated radioisotope in the diagnostic procedures due to its

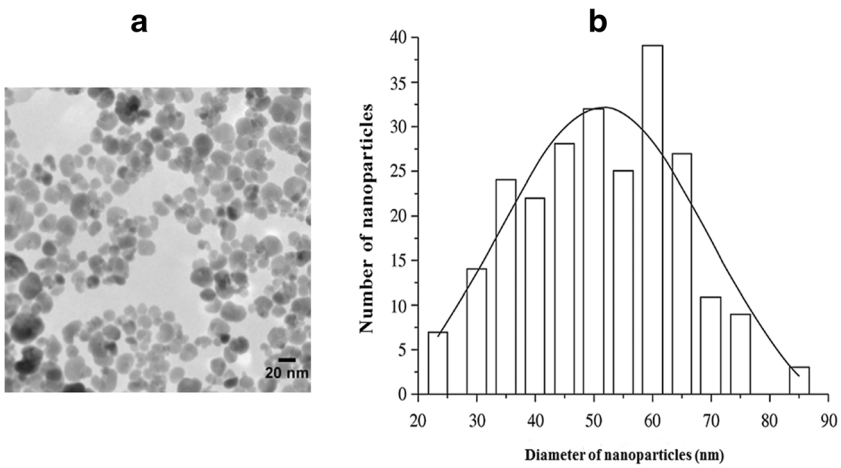

Fig. 1 Size analysis of MIONPs platform: **a** TEM image **b** Hydrodynamic size distribution

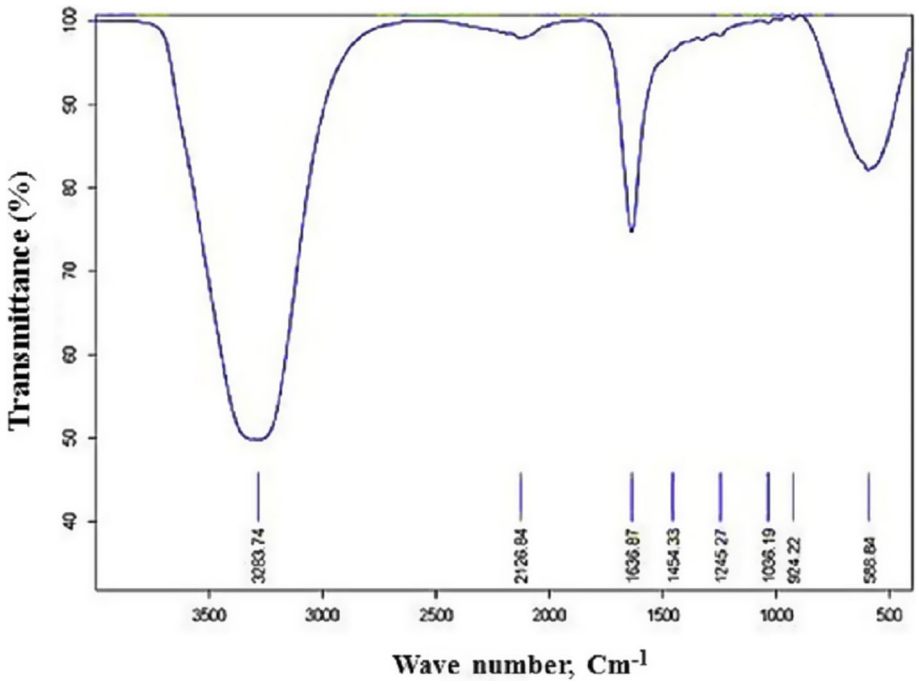

Fig. 2 The FT-IR spectra of MIONPs capped with PEG

optimal physical characteristics ($t_{1/2} \approx 6$ h, and γ energy ≈140 keV) [26]. This renders it as the key horse for the efficient diagnosis with low radiation hazard risk [26]. As mentioned above ^{99m}Tc radionuclide was entrapped inside the core of IO-PEG NPs through encapsulation method by using sonication process [27]. The radiolabeling yield at different sonication time intervals was estimated by determining the radioactivity in MIONPs precipitate after magnetic separation (Fig. 3a). The maximum radiolabeling yield (96 ± 0.83%) of ^{99m}Tc-encapsulated MIONPs was obtained after 2 h of sonication that was confirmed by paper radiochromatographic analysis using acetone as a mobile phase. With this system, ^{99m}Tc-encapsulated MIONPs were still near the spotting point while free $Na^{99m}TcO_4$ travelled to the solvent front. In electrophoresis analysis, the examined species travelled away from the application point toward the anode where free $Na^{99m}TcO_4$ appeared at 14 cm and ^{99m}Tc-encapsulated MIONPs at 4 cm.

The encapsulation of Tc-99 m radionuclide inside the core of IO-PEG NPs did not affect the hydrodynamic size depending on the re-characterization using DLS instrument.

Encapsulation efficiency (in-vitro release study)

The encapsulation efficiency or in-vitro release study of ^{99m}Tc-encapsulated MIONPs formulation was evaluated to decide the appropriate time for injection which corresponds to the lowest radionuclide leaching probability. The results showed that the ^{99m}Tc-encapsulated MIONPs formulation had appropriate encapsulation efficiency up to 8 h where only 8 ± 0.95% of encapsulated Tc-99 m had leached out (Fig. 3b).

In-vitro stability study

The in-vitro stability of the $Na^{99m}TcO_4$-encapsulated MIONPs formulation was assessed in mice serum and saline as shown in Fig. 3c and d, respectively. The radiolabeling yields were analyzed by paper radiochromatographic analysis at 0.5, 1, 2, 4, 8 and 24 h post-incubation at 37°C. The results showed sufficient radiolabeling yield of 95% up to 8 h and less than 20% of ^{99m}Tc-encapsulated MIONPs had released pertechnetate after 24 h of incubation. It is clear from this study that the ^{99m}Tc-encapsulated MIONPs formulation was stable enough in saline and mice serum, thus indicating its high in-vitro stability up to 8 h.

In-vitro cytotoxicity study

It is vital to evaluate the cytotoxic effect of the MIONPs on normal cells because they will be administrated in-vivo as drug delivery vehicles. The cytotoxic profile evaluation of MIONPs against WI-38 cell line had been demonstrated as presented in Fig. 4. The results showed that MIONPS formula had no cytotoxic effect (cell viability 100% at concentration of 0.78–25 μl/ 10^4 cells) and weak inhibitory effect at concentration of 50 and 100 μl/ 10^4 cells (cell viability 97.5 and 91.4, respectively). This weak inhibitory effect in this presented study shows a better cell viability in relation to the previously published reports on IO-NPs at the respective concentrations [28, 29].

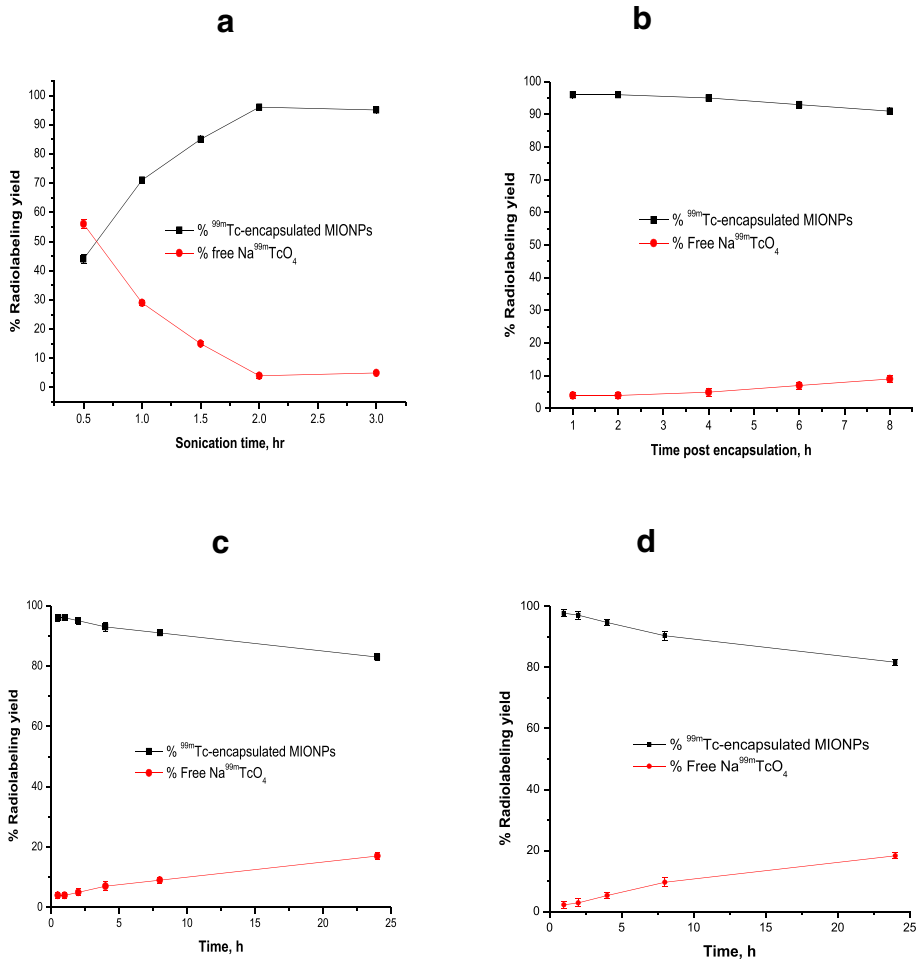

Fig. 3 Preparation and stability studies evaluation of ^{99m}Tc-encapsulated MIONPs: **a** Variation of the radiolabeling yield as a function of sonication time **b** Encapsulation efficiency **c** In-vitro stability in serum at 37 °C **d** In-vitro stability in saline at 37 °C

In-vivo biological studies

For NPs that are radiolabeled by encapsulation, it seems that the biodistribution patterns and in-vivo stability of the formed radiolabeled nanoparticles depend mainly on drug delivery vehicles [30]. The normal animal (group A) biodistribution behavior was done to evaluate the fate pattern of the prepared MIONPs formulation as shown in Fig. 5. It is demonstrated that the radiolabeled MIONPs accumulated gradually in the reticuloendothelial organs, liver and spleen, and showed maximum radioactivity accumulation of 27.35 ± 0.92 and 20.40 ± 1.35% ID/g at 60 min p.i., respectively, which demonstrate the matching pattern of NPs distribution [31]. Other organs showed low radioactivity accumulation that decreased gradually through the experimental time points. The enhanced uptake in liver and spleen may be attributed to the rapid opsonization that happens straightforwardly after I.V. administration of NPs, bringing about significant take-up by the macrophages that are available in these organs [32, 33].

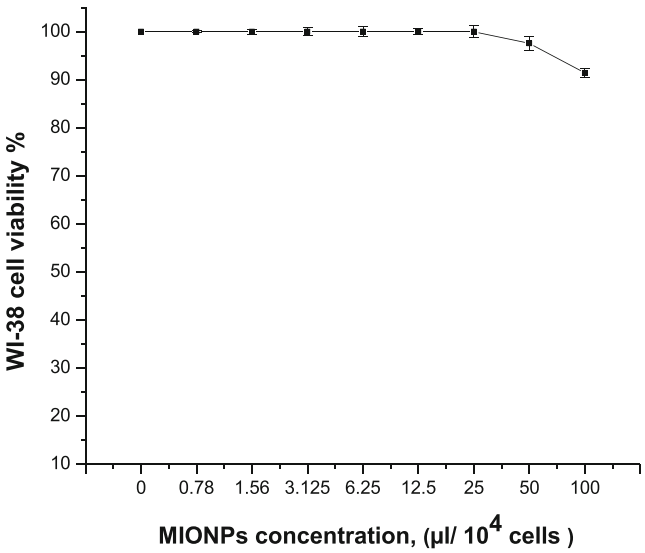

Fig. 4 Cell cytotoxicity study of different concentrations of MIONPs formulation incubated with WI-38 cells

The tumor accumulation ability of the prepared ^{99m}Tc-encapsulated MIONPs formulation in solid tumor bearing mice (group B and C) following systemic administration was studied as shown in Fig. 6a and b, respectively. For group B, the maximum radioactivity accumulation of 25.39 ± 0.57% ID/g in tumor area at 60 min post I.V. injection was observed. For group C, the results showed that tumor tissue radioactivity accumulation at 60 min post I.V. injection with physical

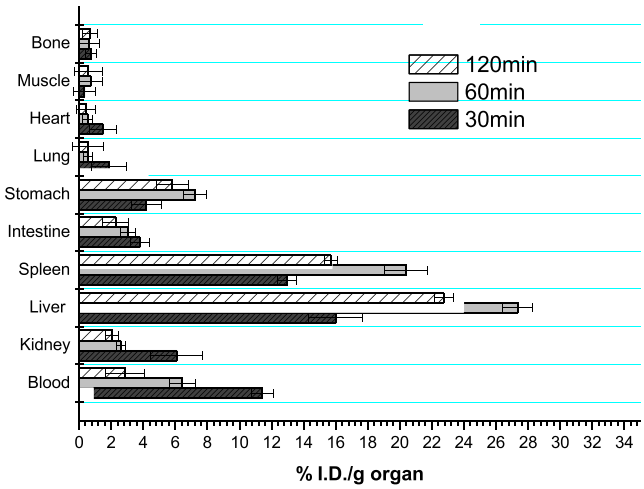

Fig. 5 In-vivo biodistribution of ^{99m}Tc-encapsulated MIONPs in normal male Swiss Albino mice at different time intervals post I.V. injection (% ID/g ± SEM, $n = 5$)

magnetic targeting increased to be 36.40 ± 0.59% ID/g which is higher than normal I.V. administration in group B. The high radioactivity accumulation and retention in tumor tissue in group B and C is due to the small sized NPs ability to passively targeted to tumor area; NPs are delivered to tumor area via highly permeable tumor vasculature and remained there because of the absence of lymphatic infiltration [34, 35]. The enhanced permeation and retention (EPR) effect is one of the pillars of nano-particulate drug delivery which provides the ability to selectively target tumor tissue. The EPR effect is exhibited by most tumors, but not in normal tissue [36, 37]. It derives from the fact that a growing tumor needs a continuous supply of blood, nutrients and oxygen in order to survive and grow larger. In order to achieve this, the tumor cells secrete vascular endothelial growth factor (VEGF) and other substances which cause angiogenesis. Angiogenesis is the recruitment of nearby blood vessels to grow new blood vessel offshoots into the developing tumor tissue. These newly constructed blood vessels however display relatively large fenestrations between the endothelial cells, about 200–780 nm, which allow NPs smaller than this cut-off to extravasate preferentially in tumor tissue [38–40]. To exit normal vasculature, sizes smaller than 1–2 nm are required. In addition to fenestrated endothelium, tumors have poor lymphatic drainage, allowing extravasated particles to stay in the tissue. A key requirement for NPs to take advantage of the EPR effect is that they circulate in the blood stream long enough for extravasation to occur [41–43]. The increased tumor accumulation and retention in group C compared

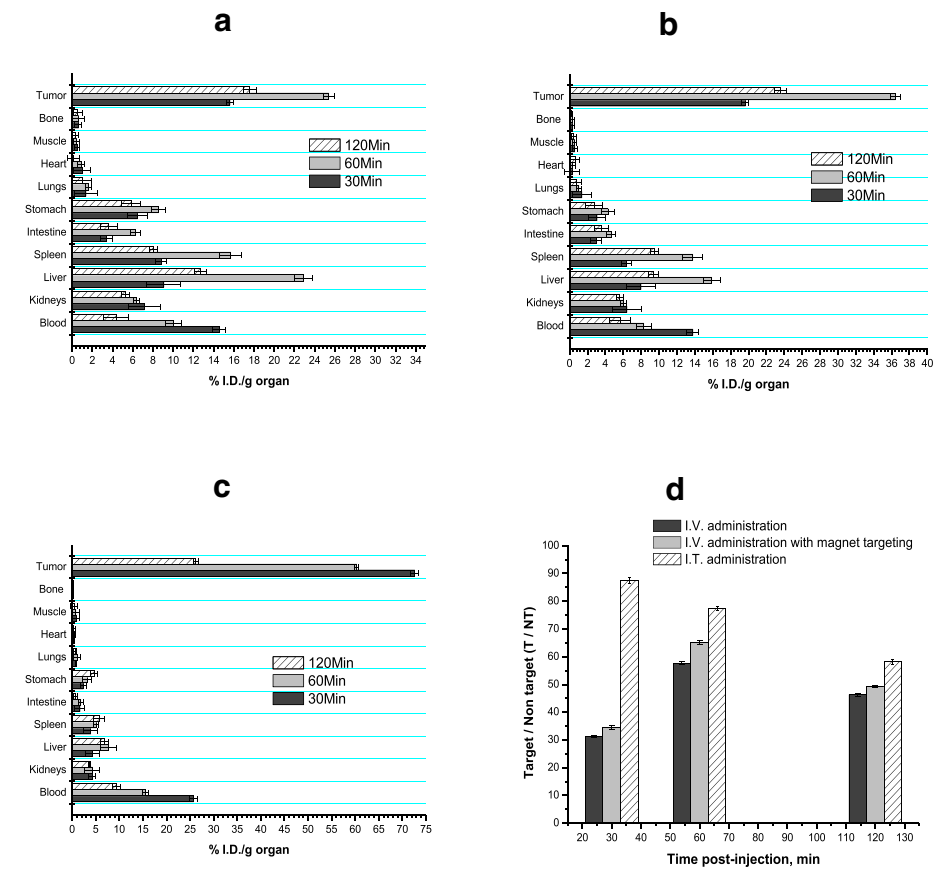

Fig. 6 In-vivo biodistribution of ^{99m}Tc-encapsulated MIONPs in solid tumor bearing mice at different time intervals post different delivery routes (% ID/g ± SEM, $n = 5$); **a** Intravenous injection; I.V. **b** I.V. with physical magnet targeting **c** Intratumoral injection; I.T. **d** T/NT ratios as a function of time

to group B could be explained by the magnetic properties of IO-NPs which develop a magnetic attraction between the injected MIONPs and the permanent magnet localized at tumor tissue.

The solid tumor bearing mice in group D were directly injected intratumorally by ^{99m}Tc-encapsulated MIONPs preparation. The biological distribution studies were performed to evaluate the radioactivity leaching from tumor tissue to the other organs. It was demonstrated that tumor tissue earned most of the radioactivity with very low leakage in the adjacent organs (Fig. 6c). The maximum tumor uptake (72.61 ± 0.82% ID/g) was observed at 30 min p.i. and dropped to 26.20 ± 0.55% ID/g at 120 min p.i. Also, it is revealed that the highest radioactivity accumulation in blood pool (25.75 ± 0.90% ID/g) was achieved at 30 min p.i. and declined to 9.39 ± 0.83% ID/g at 120 min p.i.

The biodistribution studies revealed that RES uptake in solid tumor bearing mice (group B, C and D) was lower than normal mice. It may be attributed that there are multiple methods have been investigated to avoid opsonin binding, thus increasing circulation time and increasing the carrier's ability to reach tumor cell for internalization and avoiding RES accumulation [44–46]:

1. An injectable NP has to be smaller than 100 nm to avoid phagocytic action by the RES.
2. The surface charge (−10 mV to +10 mV) also helps in increasing cellular uptake and avoid self-aggregation between NPs, also resulting in lowered RES recognition.
3. Coating the NP surface with hydrophilic polymers, such as PEG, poloxamers, or hydrophilic polysaccharides, it is possible to create a hydrated water barrier that provides good steric hindrance to the attack of phagocytes. Indeed, the presence of such macromolecules allows the prevention of opsonization thanks to this protective hydrophilic and flexible layer, preventing their interaction with blood components.
4. PEGylation simply refers to the decoration of a particle surface by the covalent surface grafting, or adsorption of PEG chains. This explains why the PEGylation strategy appears to be a key nano-technological advance, allowing PEGylated nano-carriers to overcome the opsonization and exhibit a prolonged circulation time, thus leading to an increased opportunity to reach its site of action.

All these criteria are well developed and are available in our formulation concerning 52 nm hydrodynamic size, −28 mV zeta potential and coating the NP surface with hydrophilic polymer (PEG), PEGylation.

Based on the biodistribution behavior pattern of ^{99m}Tc-encapsulated MIONPs formulation in group B, C and D, the target (tumor mass in the right thigh) to non-target (the muscle in the left thigh) (T/NT) ratios were evaluated as demonstrated in Fig. 6d. The evaluation showed great promising results in the three groups. Where, the maximum T/NT ratios of 57.70, 65.00 and 87.48 for group B, C and D were achieved at 60 min p.i.

These biologically merits of our prepared chelator free radiolabeling technique of ^{99m}Tc-encapsulated MIONPs formulation make it more potentially advanced than the already and recently published chelator mediated radiolabeled nanoformulations which reported maximum tumor uptakes in the scope of 3.65 ± 0.19 to 16.21 ± 2.56 %ID/g [25, 47–53].

Conclusion

According to our findings, nano-sized ^{99m}Tc-encapsulated MIONPs radiopharmaceutical was prepared with average particle size 24.08 nm, hydrodynamic size 52 nm and high radiolabeling yield of 96%. The radiochemical studies showed that nano-sized radiopharmaceutical could be prepared in high encapsulation efficiency of Tc-99 m radionuclide by IO-PEG NPs. The prepared ^{99m}Tc-encapsulated MIONPs formulation was in-vitro physiologically stable up to 24 h and showed no cytotoxic effect on normal cells. The in-vivo evaluation in solid tumor bearing mice demonstrated high efficacy of ^{99m}Tc-encapsulated MIONPs formulation in tumor targeting ability. The maximum tumor radioactivity accumulation (25.39 ± 0.57, 36.40 ± 0.59 and 72.61 ± 0.82% ID/g) was achieved at 60, 60 and 30 min post I.V., I.V. with permanent magnet localized at tumor region and intratumoral injection, respectively, with maximum T/NT ratios of 57.70, 65.00 and 87.48 at 60 min p.i. These preliminary merits indicate that ^{99m}Tc-encapsulated MIONPs formulation demonstrated promising highlights in the preparation of chelator free radiolabeling, encapsulation, approach and in-vivo evaluation in animal models. This encourages the future clinical investigation of ^{99m}Tc-encapsulated MIONPs formulation as molecular imaging probe for tumor diagnosis.

Acknowledgments Associate Prof. Tamer M. Sakr expresses his grateful appreciation and thanks for International Atomic Energy Authority (IAEA) for international collaboration and funding this work under CRP No. F22064.

References

1. Sakr TM, Khowessah OM, Motaleb MA, Abd El-Bary A, El-Kolaly MT, Swidan MM. I-131 doping of silver nanoparticles platform for tumor theranosis guided drug delivery. Eur J Pharm Sci. 2018;122:239–45.
2. Xing Y, Zhao J, Shi X, Conti PS, Chen K. Recent development of radiolabeled nanoparticles for PET imaging. Austin J Nanomed Nanotechnol. 2014;2(2):1016.

3. De Barros AB, Tsourkas A, Saboury B, Cardoso VN, Alavi A. Emerging role of radiolabeled nanoparticles as an effective diagnostic technique. EJNMMI Res. 2012;2(1):39.
4. Welch MJ, Hawker CJ, Wooley KL. The advantages of nanoparticles for PET. J Nucl Med. 2009;50:1743–6.
5. Goel S, Chen F, Ehlerding EB, Cai W. Intrinsically radiolabeled nanoparticles: an emerging paradigm. Small. 2014;10(19):3825–30.
6. Zhao J, Zhou M, Li C. Synthetic nanoparticles for delivery of radioisotopes and radiosensitizers in cancer therapy. Cancer Nanotechnol. 2016;7(1):9.
7. Lamb JR, Holland JP. Advanced methods for radiolabelling nanomedicines for multi-modality nuclear/MR imaging. J Nucl Med. 2018;59(3):382–9.
8. Cisneros BT, Law JJ, Matson ML, Azhdarinia A, Sevick-Muraca EM, Wilson LJ. Stable confinement of positron emission tomography and magnetic resonance agents within carbon nanotubes for bimodal imaging. Nanomedicine. 2014;9(16):2499–509.
9. Guven A, Rusakova IA, Lewis MT, Wilson LJ. Cisplatin@ US-tube carbon nanocapsules for enhanced chemotherapeutic delivery. Biomaterials. 2012;33(5):1455–61.
10. Abou DS, Pickett JE, Thorek DLJ. Nuclear molecular imaging with nanoparticles: radiochemistry, applications and translation. Br J Radiol. 2015;88:1054.
11. Maria AVW, Margarida MCO, Marcela Z, Ariane JSB, Mohammed Q, Ralph SO. Nanoradiopharmaceuticals for nanomedicine: building the future. Recent Pat Nanomed. 2014;4(2):90–4.
12. Ting G, Chang CH, Wang HE. Cancer nanotargeted radiopharmaceuticals for tumor imaging and therapy. Anticancer Res. 2009;29:4107–18.
13. Ali A, Zafar H, Zia M, Ul Haq I, Phull AR, Ali JS, et al. Synthesis, characterization, applications, and challenges of iron oxide nanoparticles. Nanotechnol Sci Appl. 2016;9:49–67.
14. Lu Q, Wei D, Zhou J, Xu J, Cheng J, Zhu J. Preparation of polymer-functionalized iron oxide nanoparticles and their biomedical properties. Chin J Chem. 2013;31:40–406.
15. Swidan MM, Sakr TM, Motaleb MA, Abd El-Bary A, El-Kolaly MT. Preliminary assessment of radioiodinated fenoterol and reproterol as potential scintigraphic agents for lung imaging. J Radioanal Nucl Chem. 2015;303:531–9.
16. Swidan MM, Sakr TM, Motaleb MA, Abd El-Bary A, El-Kolaly MT. Radioiodinated acebutolol as a new highly selective radiotracer for myocardial perfusion imaging. J Label Compd Radiopharm. 2014;57:593–9.
17. Sakr TM, Ibrahim AB, Fasih TW, Rashed HM. Preparation and biological profile of 99mTc-lidocaine as a cardioselective imaging agent using 99mTc eluted from 99Mo/99mTc generator based on Al-Mo gel. J Radioanal Nucl Chem. 2017;314(3):2091–8.
18. Radovic M, Calatayud MP, Goya GF, Ibarra MR, Antic B, Spasojevic V, et al. Preparation and in vivo evaluation of multifunctional 90Y-labeled magnetic nanoparticles designed for cancer therapy. J Biomed Mater Res A. 2015;103(1):126–34.
19. Liu XL, Fan HM, Yi JB, Yang Y, Choo ESG, Xue JM, et al. Optimization of surface coating on Fe_3O_4 nanoparticles for high performance magnetic hyperthermia agents. J Mater Chem B. 2012;22:8235–44.
20. Sinha N, Cifter G, Sajo E, Kumar R, Sridhar S, Nguyen PL, et al. Brachytherapy application with in situ dose painting administered by gold nanoparticle eluters. Int J Radiat Oncol Biol Phys. 2015;91:385–92.
21. Kong L, Hu J, Qin D, Yan P. Interaction of Ifosfamide-loaded superparamagnetic iron oxide nanoparticles with human serum albumin-a biophysical study. J Pharm Innov. 2015;10:13–20.
22. Mondini S, Cenedese S, Marinoni G, Molteni G, Santo N, Bianchi CL, et al. One-step synthesis and functionalization of hydroxyl-decorated magnetite nanoparticles. J Colloid Interface Sci. 2008;322:173–9.
23. Khayatian G, Hassanpoor S, Azar ARJ, Mohebbi S. Spectrophotometric determination of trace amounts of uranium(VI) using modified magnetic iron oxide nanoparticles in environmental and biological samples. J Braz Chem Soc. 2013;24:1808–17.
24. Mirshojaei SF, Ahmadi A, Avila EM, Reynoso MO, Perez HR. Radiolabelled nanoparticles: novel classification of radiopharmaceuticals for molecular imaging of cancer. J Drug Target. 2016;24(2):91–101.
25. Tsiapa I, Efthimiadou EK, Fragogeorgi E, Loudos G, Varvarigou AD, Bouziotis P, et al. ^{99m}Tc-labeled aminosilane-coated iron oxide nanoparticles for molecular imaging of $\alpha_v\beta_3$-mediated tumor expression and feasibility for hyperthermia treatment. J Colloid Interface Sci. 2014;433:163–75.
26. Banerjee S, Pillai MR, Ramamoorthy N. Evolution of Tc-99m in diagnostic radiopharmaceuticals. Semin Nucl Med. 2001;31:260–77.
27. Matson ML, Villa CH, Ananta JS, Law JJ, Scheinberg DA, Wilson LJ. Encapsulation of α-particle-emitting $^{225}Ac^{3+}$ ions within carbon nanotubes. J Nucl Med. 2015;56(6):897–900.
28. Gonzales M, Mitsumori LM, Kushleika JV, Rosenfeld ME, Krishnan KM. Cytotoxicity of iron oxide nanoparticles made from the thermal decom-position of organometallics and aqueous phase transfer with Pluronic F127. Contrast Media Mol Imaging. 2010;5(5):286–93.
29. Hoskins C, Cuschieri A, Wang L. The cytotoxicity of polycationic iron oxide nanoparticles: common endpoint assays and alternative approaches for improved understanding of cellular response mechanism. J Nanobiotechnology. 2012;10:15.
30. Bao A, Goins B, Klipper R, Negrete G, Phillips WT. Direct ^{99m}Tc labeling of pegylated liposomal doxorubicin (Doxil) for pharmacokinetic and non-invasive imaging studies. J Pharmacol Exp Ther. 2004;308:419–25.
31. Amirkhizi AA, Banaem LM, Allaf MA, Sadjadi S, Daha FJ. Development of dendrimer encapsulated Radio-Ytterbium and biodistributionin tumor bearing mice. IEEE Trans NanoBiosci. 2016;15(6):549–54.
32. Psimadas D, Bouziotis P, Georgoulias P, Valotassiou V, Tsotakos T, Loudos G. Radiolabeling approaches of nanoparticles with ^{99m}Tc. Contrast Media Mol Imaging. 2013;8:333–9.
33. Zhang G, Yang Z, Lu W, Zhang R, Huang Q, Tian M, et al. Influence of anchoring ligands and particle size on the colloidal stability and in vivo biodistribution of polyethylene glycol-coated gold nanoparticles in tumor-xenografted mice. Biomaterials. 2009;30(10):1928–36.
34. Shi J, Kantoff PW, Wooster R, Farokhzad OC. Cancer nanomedicine: progress, challenges and opportunities. Nat Rev Cancer. 2017;17:20–37.
35. Thakor AS, Gambhir SS. Nanooncology: the future of cancer diagnosis and therapy. CA Cancer J Clin. 2013;63:395–418.
36. Matsumura Y, Maeda H. A new concept for macromolecular therapeutics in cancerchemotherapy: mechanism of tumoritropic accumulation of proteins and the antitumor agent smancs. Cancer Res. 1986;46(12):6387–92.
37. Maeda H. The enhanced permeability and retention (EPR) effect in tumor vasculature: the key role of tumor-selective macromolecular drug targeting. Adv Enzym Regul. 2001;41:189–207.
38. Folkman J. What is the evidence that tumors are angiogenesis dependent. J Natl Cancer Inst. 1990;82(1):4.
39. Folkman J. Angiogenesis in cancer, vascular, rheumatoid and other disease. Nat Med. 1995;1(1):27.
40. Folkman J. Tumor angiogenesis-therapeutic implications. N Engl J Med. 1971;285(21):1182–6.

41. Hobbs SK, Monsky WL, Yuan F, Roberts WG, Griffith L, Torchilin VP, et al. Regulation of transport pathways in tumor vessels: role of tumor type and microenvironment. Proc Natl Acad Sci U S A. 1998;95(8):4607–12.
42. Venturoli D, Rippe B. Ficoll and dextran vs. globular proteins as probes for testing glomerular permselectivity: effects of molecular size, shape, charge, and deformability. Am J Physiol Renal Physiol. 2005;288(4):F605–13.
43. Konno T, Maeda H, Iwai K, Maki S, Tashiro S, Uchida M, et al. Selective targeting of anticancer drug and simultaneous image enhancement in solid tumors by arterially administered lipid contrast-medium. Cancer. 1984;54(11):2367–74.
44. Moghimi SM, Szebeni J. Stealth liposomes and long circulating nanoparticles: critical issues in pharmacokinetics, opsonization and protein-binding properties. Prog Lipid Res. 2003;42(6):463–78.
45. Moghimi SM, Hunter AC, Murray JC. Long-circulating and target-specific nanoparticles: theory to practice. Pharmacol Rev. 2001;53(2):283–318.
46. Gref R, Luck M, Quellec P, Marchand M, Dellacherie E, Harnisch S, et al. Stealth' corona-core nanoparticles surface modified by polyethylene glycol (PEG): influences of the corona (PEG chain length and surface density) and of the core composition on phagocytic uptake and plasma protein adsorption. Colloids Surf B Biointerfaces. 2000;18(3–4):301–13.
47. Yang X, Hong H, Grailer JJ, Rowland IJ, Javadi A, Hurley SA, et al. cRGD-functionalized, DOX-conjugated, and ^{64}Cu-labeled superparamagnetic iron oxide nanoparticles for targeted anticancer drug delivery and PET/MR imaging. Biomaterials. 2011;32(17):4151–60.
48. Morales-Avila E, Ferro-Flores G, Ocampo-Garcia BE, Leon-Rodriguez LM, Santos-Cuevas CL, Garcia-Becerra R, et al. Multimeric system of 99mTc-labeled gold nanoparticles conjugated to c[RGDfK(C)] for molecular imaging of tumor α(v)β(3) expression. Bioconjug Chem. 2011;22:913–22.
49. Liu Z, Cai W, He L, Nakayama N, Chen K, Sun X, et al. In vivo biodistribution and highly efficient tumour targeting of carbon nanotubes in mice. Nat Nanotechnol. 2007;2:47–52.
50. Lahooti A, Sarkar S, Saligheh-Rad H, Gholami A, Nosrati S, Muller RN, et al. PEGylated superparamagnetic iron oxide nanoparticles labeled with 68Ga as a PET/MRI contrast agent: a biodistribution study. J Radioanal Nucl Chem. 2017;311:769–74.
51. Natarajan A, Xiong CY, Gruettner C, DeNardo GL, DeNardo SJ. Development of multivalent radioimmunonanoparticles for cancer imaging and therapy. Cancer Biother Radiopharm. 2008;23:82–91.
52. Hu G, Lijowski M, Zhang H, Partlow KC, Caruthers SD, Kiefer G, et al. Imaging of Vx-2 rabbit tumors with alpha (nu) beta3-integrin-targeted 111In nanoparticles. Int J Cancer. 2007;120(9):1951–7.
53. Tsoukalas C, Psimadas D, Kastis GA, Koutoulidis V, Harris AL, Paravatou-Petsotas M, et al. A novel metal-based imaging probe for targeted dual-modality SPECT/MR imaging of angiogenesis. Front Chem. 2018;6:224.